Chapter 5

A Large-Area Search for New Brown Dwarfs and Low Mass Stars in Upper Scorpius[1]

I present a wide-field photometric survey covering ∼150 deg^2 toward the Upper Scorpius OB association. Data in the BRI bands (converted to gri) taken with the Quest-2 camera on the Palomar 48-inch telescope were combined with the 2MASS JHK_S survey and used to select candidate pre-main sequence stars. Follow-up spectroscopy with the Palomar 200-inch telescope and the CTIO 4-m telescope of 243 candidate late-type members identified 145 stars that have surface gravity signatures consistent with association membership. Twelve of the 145 PMS stars identified exhibit Hα emission sufficient for accretion. From the optical/near-infrared photometry and derived spectral types, I construct an HR diagram for the new members and find 56 likely brown dwarfs, more than doubling the known substellar population of the Upper Scorpius OB association. From analysis of all observed PMS candidates compared to those determined to be association members, I conclude that the northern part of USco's low mass population shares a common spatial distribution with the high mass members, and find no evidence for spatial segregation.

[1]A modified version of this chapter has been published previously as Slesnick, Carpenter, & Hillenbrand 2006, AJ, 131, 3016. The current work has been updated to reflect new spectral observations taken after the time of original publication.

5.1 Motivation

The Upper Scorpius OB Association (USco) is the closest (145 pc; de Zeeuw et al. 1999) young OB association to the Sun with 120 known high mass Hipparcos stars. At an age of ∼5 Myr (Preibisch et al., 2002), this cluster is at an intermediate age between very young star forming regions and older open clusters where samples are sparser and studies of processes such as circumstellar disk dissipation are critical. Recent mid-infrared work by Mamajek et al. (2004) and Silverstone et al. (2006) indicates that by ∼10 Myr dust is removed from the inner few AU of circumstellar disks for $\gtrsim$85% of stars, whereas ∼80% of young 1 Myr stars in Taurus still retain their disks at these radii (Kenyon & Hartmann 1995; Skrutskie et al. 1990). This evolution in circumstellar material corresponds to the stage when planets are thought to be forming. Meteoritic evidence suggests the timescale for dissipation of our own solar system's nebula was on order of $\sim 10^7$ yr (Podosek & Cassen, 1994). Further, discovery of ^{60}Fe in meteorites argues that short-lived radionuclides were injected into the solar system's early protoplanetary disk from the explosion of a nearby supernovae (Desch & Ouellette 2005; Tachibana & Huss 2003). This evidence strongly suggests that our solar system was formed in an OB association similar to USco. Therefore, if we are to understand our own earth's origins, we must study the evolution of OB association members during planet-building stages.

A major difficulty faced by studies of the USco region is that the Hipparcos members alone span >200 deg^2 on the sky. Obtaining a complete census of the association's low mass population is thus a formidable task as one must identify faint objects over a very large spatial region. While there exist several techniques to identify young stars not associated with molecular gas, many of them are also accretion diagnostics. For example, a common method is to search for strong Hα emission (Ardila et al., 2000) produced in outflow or accretion flows (see §5.3.3), or near-infrared excess emission associated with warm inner accretion disks. While accretion can terminate over a wide range in age (1–10 Myr), the median lifetime of optically thick accretion disks is closer to 2–3 Myr (Haisch et al. 2001; Hillenbrand 2005). Therefore, surveys to look

for accretion signatures alone will not garner a full census of a 5 Myr association.

Enhanced chromospheric and coronal activity can last well beyond accretion timescales. This activity is linked with X-ray emission (Ku & Chanan 1979; Feigelson & Decampli 1981) though the exact cause of this phenomenon is still not fully understood (Preibisch et al., 2005). Many previous large-scale efforts in USco have successfully utilized Einstein data (Walter et al., 1994) or the ROSAT All Sky Survey (RASS; Preibisch et al. 1998; Preibisch & Zinnecker 1999) to identify hundreds of low and intermediate mass association members. However, neither the Einstein observations nor the RASS were sensitive enough to detect faint X-ray emission from the lowest mass stars and brown dwarfs.

Recently, deep, multicolor imaging surveys combined with spectroscopic follow-up have proved successful in identifying both the youngest classical T Tauri-type objects and more evolved very low mass stars and brown dwarfs in a variety of young regions. Young PMS objects still undergoing contraction towards the main sequence are redder and more luminous than their main sequence counterparts. Spectroscopic follow-up observations allow assessment of surface gravity diagnostics which can be used to distinguish young PMS stars from reddened field dwarfs and background giants. Previous imaging and spectroscopic surveys in USco include work by Preibisch et al. (2001) and Preibisch et al. (2002) who selected candidate association members based on optical magnitudes and colors obtained from photographic plates in the United Kingdon Schmidt Telescope survey fields. Their spectroscopic survey of 700 candidates over 9 deg^2 using the 2dF multifiber spectrograph yielded 166 new PMS stars based on the presence of lithium in their spectra. Martín et al. (2004) selected candidate young objects from the DENIS I, J survey and obtained spectra of 36 targets. Of these 28 were confirmed to be new low mass association members based on surface gravity diagnostics. Ardila et al. (2000) used R, I, Z photographic photometry to identify candidate members within an 80'×80' area of the association. Spectroscopic data were obtained for 22 candidates, 20 of which were determined to exhibit Hα emission indicating possible membership. Thus far, over 300 low mass (M <0.6 M$_\odot$) members have been identified in USco through X-rays, Hα emission,

photometry and/or spectroscopy. However most searches have been limited to small subregions or bright objects. Given the USco upper IMF, and assuming the high and low mass objects share the same spatial distribution, Preibisch et al. (2002) estimate the entire USco region should contain >1500 young, low mass objects with M <0.6 $M_{\odot}$, most of which are yet to be discovered.

5.2 Observations

Building on previous work in this region, I have completed a large-area optical *gri* photometric survey of ∼150 deg^2 in and near USco. Details of the photometric survey were given in chapter 2. My primary goal in USco is to significantly expand the number of known intermediate-age, ∼5–10 Myr-old low mass stars and brown dwarfs. Identifying large samples of objects at this age is critical for our understanding of early stellar evolution and planet formation. Usco is the ideal region to conduct such a survey because it contains the largest (>1500 objects) nearby (<300 pc) population of low mass intermediate-age PMS stars, most of which have not yet been uncovered. In chapter 3, I combined the Quest-2 photometric data with 2MASS JHK_S photometry to select candidate PMS stars, and presented newly obtained spectral data for 243 candidates discussed here. These candidates represent all stars observed at either Palomar or CTIO which meet all of the selection criteria outlined in §3.1.

All spectral analysis was carried out as outlined in chapter 3. Figure 5.1 shows spectral indices for 167 PMS spectral candidates in the USco region observed at Palomar. In the left panel I find fourteen outliers to sit below the main locus of data points. In all cases, the star is confirmed to exhibit low gravity signatures (§3.2.2) and I attribute the position in figure 5.1 to a small amount of veiling or reddening present in its spectra (§3.2.3). As shown in the right panel of figure 5.1, a large fraction (∼65%) of the candidate objects have measured Na-8190 indices consistent with their having surface gravity less than that of field dwarfs at similar spectral types. Note that because both program stars and most standard stars were observed at similar high airmasses in this region, there does not exist a systematic shift in the Na-8190

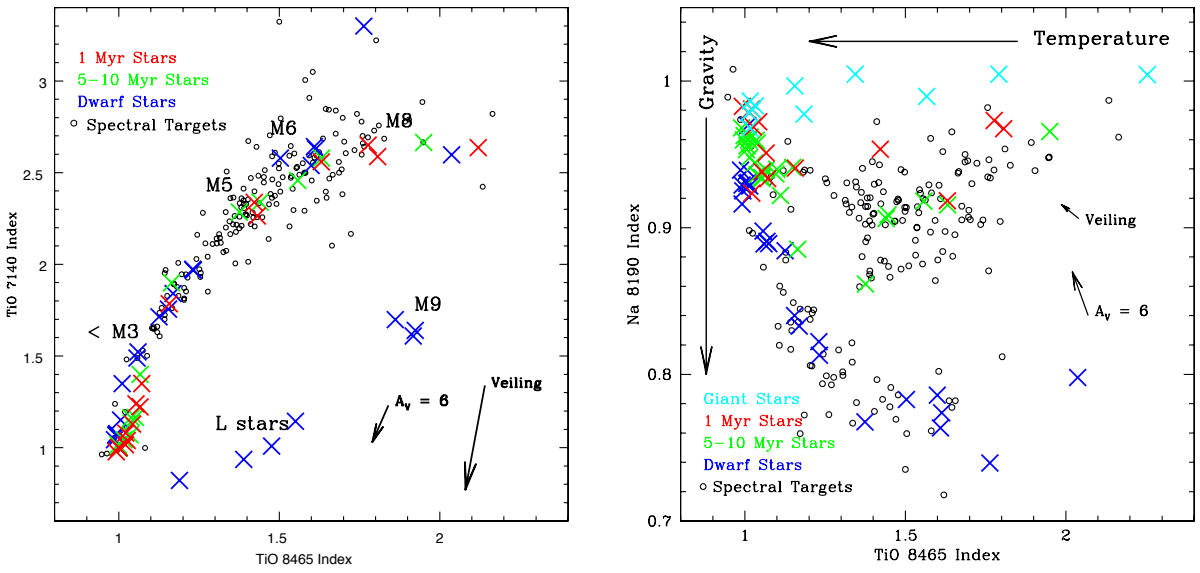

Figure 5.1 The left panel shows temperature-sensitive TiO-7140 vs. TiO-8465 indices; the right panel shows the TiO-8465 index vs. the gravity sensitive Na-8190 index. In both panels, blue X's represent measured indices for field dwarfs and members of the Hyades (∼650 Myr), Pleiades (∼115 Myr) and AB Dor (∼75–150 Myr) associations. Green X's show measured indices for intermediate-age spectral standards from Beta Pic (∼11 Myr), TW Hya (∼8 Myr), and Upper Sco (∼5 Myr). Red X's show measured indices for young Taurus members (∼1–2 Myr). Cyan X's in the right panel represent measured indices for giant standard stars. In both panels, black symbols are measured indices for USco PMS candidates observed at Palomar. The effects of extinction and veiling are shown as vectors (see §3.2.3).

index between the two populations as was the case in Taurus (chapter 4).

Of the 243 objects with spectra presented here, 76 were observed with the hydra multifiber spectrograph on the 4-m telescope at CTIO. These spectra have not been flux calibrated due to the intrinsic difficulties with this process for spectra taken through fibers. Thus, I cannot use quantitative index measurements for spectral classification, and all spectra were classified visually in relation to each other and to spectral standards taken during the observing run.

Table 5.1 lists optical and near-infrared 2MASS photometry, measured spectral indices (for Palomar spectra), spectral types and Hα equivalent widths for all USco

members discovered in my work. Seventeen of the 145 PMS stars identified here have been previously discussed in the literature, including 12 with previous spectral type determinations. When present, an alternative ID and spectral type is also given.

Table 5.1. Measured quantities for new PMS stars in USco

ID[a]	g	r	i	J[c]	H[c]	K_S[c]	TiO-7140	TiO-8165	Na-8195	SpType[d]	$W(H\alpha)$ [Å]	Otherid/Sptype
SCH J15560497-21064632		20.19	17.72	14.12	13.41	12.97	2.88	1.94	0.94	M7	-16.5	DENIS-P J155605.0-210646/M7[e]
SCH J15561978-24232936		18.17	16.18	13.36	12.74	12.48				M4.5	-9.2	
SCH J15574757-24441236	19.02	17.37	15.81	12.98	12.36	12.05				M4	-8.8	
SCH J15582337-21515908[b]	18.71			12.24	11.59	11.28	2.21	1.36	0.94	M4.75	-9.4	
SCH J15582566-18260865	19.59	18.17	16.03	12.92	12.20	11.79	2.55	1.57	0.92	M6	-20.2	
SCH J15583162-24025411		18.05	16.02	13.16	12.51	12.20	1.95	1.25	0.93	M4.5	-7.6	
SCH J15584812-21413426	20.23	18.53	16.50	13.48	12.87	12.51	2.39	1.42	0.87	M5.5	-10.8	
SCH J15594802-22271650		19.83	17.49	14.24	13.56	13.16	2.78	1.90	0.93	M7.5	-15.2	
SCH J15595868-18365205		19.15	16.76	13.43	12.76	12.40	2.48	1.53	0.91	M5.5	-14.8	
SCH J16002669-20563190	20.00	18.33	16.39	13.46	12.89	12.50				M4.5	-16.6	UScoCTIO 112/M5.5[h]
SCH J16014156-21113855	19.05	17.54	15.76	12.74	12.04	11.68				M4	-79.2	
SCH J16014768-24410152		19.08	16.92	13.87	13.27	13.00	2.44	1.45	0.86	M5	-16.0	
SCH J16024143-22484204		18.29	16.19	13.04	12.42	11.99	2.48	1.56	0.91	M5.5	-18.4	UScoCTIO 102[h]
SCH J16024576-23045102	18.91	17.46	15.32	12.46	11.84	11.50	2.33	1.38	0.87	M5	-9.6	[PBB2002] USco J160245.7-230450/M6[f]
SCH J16033470-18293060	19.38	17.63	15.50	12.51	11.83	11.48	2.21	1.38	0.91	M5	-36.6	DENIS-P J160334.7-182930/M5[e]
SCH J16034029-23352386		16.39	14.74	12.26	11.62	11.32				M4	-5.3	
SCH J16035651-23572517	19.91	18.43	16.49	13.60	13.01	12.67				M4.5	-10.3	
SCH J16040453-23463795	17.19	15.76	14.15	11.74	11.04	10.73	1.81	1.20	0.93	M4	-4.0	
SCH J16044303-23182620		19.50	17.17	13.81	13.19	12.85	2.72	1.79	0.90	M6.5	-18.0	UScoCTIO 1102[h]
SCH J16051829-17562092	17.07	15.65	14.04	11.64	10.98	10.68	1.66	1.11	0.93	M4	-5.4	
SCH J16053077-22462016		19.47	17.17	13.78	13.18	12.78	2.84	1.65	0.89	M6	-17.8	
SCH J16054416-21550566		16.79	14.80	11.90	11.28	10.94	2.35	1.40	0.90	M5	-9.4	
SCH J16060391-20564497		19.43	17.18	13.52	12.90	12.47	2.77	1.89	0.95	M7	-159.0	DENIS-P J160603.9-205644/M7.5[e]
SCH J16072239-20115852	19.27	17.73	15.76	12.70	12.02	11.58	2.37	1.48	0.93	M5.5	-14.2	[PBB2002] USco J160722.4-201158/M5[f]

Table 5.1 (cont'd)

ID[a]	g	r	i	J[c]	H[c]	K_S[c]	TiO-7140	TiO-8165	Na-8195	SpType[d]	$W(H\alpha)$ [Å]	Otherid/Sptype
SCH J16072640-21441727		20.21	17.95	14.66	14.02	13.67	2.36	1.64	0.88	M6	-10.7	
SCH J16075565-24432714		18.68	16.66	13.83	13.13	12.71	2.13	1.46	0.90	M5.5	-47.3	
SCH J16075850-20394890		19.12	16.91	13.59	12.95	12.58	2.47	1.53	0.89	M6	-14.9	
SCH J16081081-22294303		17.55	15.61	12.61	11.99	11.67				M5	-49.0	
SCH J16083646-24453053	16.64	15.32	13.79	11.59	10.94	10.73				M3.5	-12.0	
SCH J16083658-18024994		18.41	16.14	12.78	12.21	11.75	2.59	1.75	0.93	M6.5	-16.6	
SCH J16084058-22255726	19.78	18.29	16.52	14.09	13.46	13.22				M4	-2.6	
SCH J16084170-18561077	19.44	17.69	15.50	12.22	11.58	11.21	2.55	1.60	0.92	M6	-10.1	[PBB2002] USco J160841.7-185610/M6[f]
SCH J16085870-24493641	18.02	16.54	14.86	12.31	11.66	11.41				M4	-7.1	
SCH J16090451-22245259		19.03	16.49	13.01	12.36	11.99	2.75	1.81	0.95	M7	-17.1	
SCH J16090511-24262843		15.87	14.29	11.96	11.26	10.98				M4	-5.9	
SCH J16090771-23395430	18.57	17.06	15.09	12.08	11.44	11.13	2.30	1.39	0.92	M5	-15.7	
SCH J16090883-22174699	19.34	17.71	15.64	12.97	12.33	12.07				M5	-14.4	
SCH J16091837-20073523		17.96	16.11	13.00	12.37	12.01				M7.5	-15.5	
SCH J16092137-21393452	18.71	16.96	14.98	11.98	11.38	11.02	2.25	1.43	0.92	M5.5	-24.5	
SCH J16093018-20595409		19.41	17.30	13.99	13.35	12.98	2.59	1.53	0.89	M6	-11.1	
SCH J16093707-20525337	19.50	17.80	15.86	12.90	12.25	11.97	2.28	1.33	0.91	M4.75	-5.7	
SCH J16095217-21362826	20.24	18.33	16.05	12.56	11.96	11.56	2.66	1.76	0.94	M7	-26.2	
SCH J16095307-19481704		18.12	16.00	12.80	12.16	11.76	2.58	1.60	0.91	M6	-21.7	
SCH J16095695-22120300		18.72	16.49	13.62	13.03	12.66	2.64	1.53	0.90	M5.5	-8.9	
SCH J16095991-21554293		19.84	17.50	14.30	13.64	13.30	2.49	1.57	0.89	M6.5	-17.4	
SCH J16100129-21522466[b]	19.75			12.63	12.06	11.70	2.53	1.55	0.91	M5.5	-12.0	
SCH J16100541-19193636		20.75	18.13	14.21	13.43	12.70	2.55	1.68	0.94	M6	-49.8	DENIS-P J161005.4-191936/M7[e]
SCH J16100751-18105666		18.34	16.06	12.74	12.15	11.75	2.82	1.74	0.90	M6	-15.9	DENIS-P J161007.5-181056/M6[e]

Table 5.1 (cont'd)

ID[a]	g	r	i	J[c]	H[c]	K_S[c]	TiO-7140	TiO-8165	Na-8195	SpType[d]	$W(H\alpha)$ [Å]	Otherid/Sptype
SCH J16101190-21015540	20.24	18.80	16.77	13.78	12.99	12.57	2.41	1.54	0.91	M5.5	-14.6	
SCH J16102990-24035024	18.97	17.42	15.59	12.92	12.33	12.01				M4.5	-10.0	
SCH J16103525-20291714	19.53	17.77	15.77	12.69	12.04	11.71	2.25	1.37	0.91	M5	-12.5	
SCH J16103876-18292353		19.87	17.63	13.96	13.16	12.64	2.29	1.57	0.96	M6	-80.3	
SCH J16104635-18405996	19.35	17.64	15.56	12.70	11.81	11.26	1.97	1.25	0.93	M4.5	-8.8	[PBB2002] USco J161046.3-184059/M4[f]
SCH J16105500-21261422	19.71	18.19	16.03	12.77	12.10	11.77	2.59	1.59	0.90	M6	-27	
SCH J16105727-23595416	18.68	17.31	15.57	12.86	12.21	11.91				M4	-7.4	
SCH J16110144-19244914		18.44	16.43	13.35	12.71	12.36	2.27	1.39	0.90	M5	-9.3	
SCH J16110739-22285027	19.26	17.64	15.44	12.31	11.72	11.32	2.29	1.54	0.92	M6.25	-139.1	
SCH J16111711-22171749		20.37	17.97	14.34	13.73	13.25	2.68	1.82	0.94	M7.5	-20.8	
SCH J16112629-23400611		18.33	16.42	13.44	12.82	12.47	2.32	1.49	0.90	M5.5	-7.1	
SCH J16112959-19002921		19.76	17.35	13.67	12.90	12.44	2.49	1.68	0.94	M6	-20.4	
SCH J16114735-22420649		18.46	16.41	13.49	12.82	12.53	2.33	1.37	0.89	M5	-13.1	
SCH J16115737-22150691		18.75	16.70	13.73	13.10	12.73	2.26	1.39	0.90	M5	-8.6	
SCH J16121044-19322708	19.03	17.19	15.30	12.23	11.59	11.23	2.31	1.38	0.92	M5	-12.8	
SCH J16121188-20472698		19.39	17.09	13.66	13.02	12.60	2.69	1.77	0.93	M6.5	-8.1	
SCH J16122764-24064850	19.54	17.85	15.88	12.89	12.29	11.93				M7	-13.5	
SCH J16123459-24583447	18.37	16.87	14.83	11.94	11.36	11.04	2.26	1.36	0.91	M4.75	-13.5	
SCH J16123758-23492340		19.10	17.00	13.93	13.28	12.91	2.47	1.51	0.87	M6	-15.8	
SCH J16124506-23053043		18.70	16.52	13.48	12.87	12.46	2.48	1.43	0.87	M5.5	-9.8	
SCH J16124692-23384086		19.25	16.98	13.65	13.02	12.62	2.66	1.70	0.90	M6	-14.7	
SCH J16125723-24280145		17.46	15.68	12.93	12.28	11.95				M4	-11.8	
SCH J16130306-19293234		18.85	16.75	13.45	12.76	12.35	2.60	1.54	0.92	M5.5	-7.3	
SCH J16130764-17035233		18.95	16.83	13.71	13.02	12.71	2.32	1.46	0.90	M5.5	-7.9	

Table 5.1 (cont'd)

ID[a]	g	r	i	J[c]	H[c]	K_S[c]	TiO-7140	TiO-8165	Na-8195	SpType[d]	$W(H\alpha)$ [Å]	Otherid/Sptype
SCH J16131212-23050329		19.87	17.43	14.05	13.44	13.00	2.62	1.73	0.90	M6.5	-13.4	
SCH J16131857-15293460	17.87	16.50	14.49	11.68	11.05	10.76	2.23	1.34	0.93	M4.75	-14.4	
SCH J16132576-17373542	17.98	16.48	14.83	12.32	11.69	11.40	1.72	1.14	0.91	M4	-5.3	
SCH J16132809-19245288	19.87	18.22	16.16	12.92	12.26	11.91	2.46	1.47	0.91	M6	-14.7	[PBB2002] USco J161328.0-192452/M5[f]
SCH J16141351-22445788		16.76	15.02	12.37	11.72	11.42				M4	-5.4	
SCH J16141484-24270844		17.83	15.60	12.47	11.85	11.48				M7	-17.6	
SCH J16141974-24284053		19.46	17.13	13.81	13.15	12.76	2.59	1.61	0.88	M6	-16.4	
SCH J16143286-22421358		20.54	17.87	14.23	13.66	13.24	2.77	1.75	0.98	M6.5	-23.6	
SCH J16150524-24593542		17.70	15.58	12.55	11.90	11.48	2.01	1.40	0.92	M5	-38.4	
SCH J16151115-24201556		19.68	17.46	14.23	13.58	13.17	2.33	1.43	0.90	M6	-10.9	
SCH J16151360-23042637		20.35	18.18	14.81	14.19	13.91	2.69	1.75	0.87	M6.5	-35.9	
SCH J16153915-191700073	19.03	17.32	15.09	11.68	10.84	10.43	2.11	1.31	0.93	M4.75	-9.3	
SCH J16155508-24443677		19.18	16.81	13.39	12.74	12.28	2.48	1.66	0.93	M6	-15.8	
SCH J16162396-24083016	19.69	17.67	16.02	13.15	12.51	12.13				M5	-17.5	DENIS-P J161624.0-240830/M5.5[e]
SCH J16162599-21122315		19.42	17.34	14.26	13.63	13.30	2.35	1.38	0.89	M5	-11.3	
SCH J16163504-20575551	19.04	17.26	15.29	12.22	11.63	11.29	2.38	1.47	0.91	M5.5	-17.6	
SCH J16164538-23334143		18.79	16.77	13.77	13.15	12.81	2.27	1.39	0.86	M5	-17.1	
SCH J16165160-20485398	18.13	16.49	14.78	12.11	11.43	11.13				M4	-5.0	
SCH J16171901-21371312		18.78	16.65	13.48	12.86	12.54	2.52	1.49	0.91	M5.5	-13.4	
SCH J16172504-23503799		19.40	17.20	13.74	13.01	12.63	2.25	1.44	0.87	M5	-12.0	
SCH J16173105-20504715		18.83	16.49	13.03	12.36	12.02				M7	-34.8	
SCH J16173238-20403653		20.83	18.18	14.34	13.68	13.19	2.60	1.70	0.92	M6	-24.6	
SCH J16173788-21191618	18.41	16.84	14.93	12.23	11.54	11.26				M4	-8.7	
SCH J16174368-21115536	20.36	18.67	17.04	14.47	13.68	13.35				M4	-4.7	

Table 5.1 (cont'd)

ID[a]	g	r	i	J[c]	H[c]	K_S[c]	TiO-7140	TiO-8165	Na-8195	SpType[d]	$W(H\alpha)$ [Å]	Otherid/Sptype
SCH J16174540-23533618		19.88	17.44	14.05	13.31	12.95	2.83	1.67	0.91	M6	-15.5	
SCH J16181201-24133263	19.29	17.77	15.70	12.69	11.93	11.59				M5	-21.7	
SCH J16181567-23470847		18.55	16.18	12.42	11.51	10.97	2.32	1.39	0.94	M5.5	-16.3	
SCH J16181601-24372688	18.54	16.75	14.70	11.67	10.92	10.59				M4	-16.1	
SCH J16181906-20284815	19.13	17.36	15.38	12.39	11.50	10.95	2.14	1.31	0.91	M4.75	-11.3	
SCH J16182501-23381068		19.50	17.19	13.72	12.88	12.44	2.06	1.32	0.91	M5	-9.2	
SCH J16183144-24195229		20.22	17.76	14.15	13.46	12.97	2.45	1.60	0.87	M6.5	-11.4	
SCH J16183620-24253332	18.36	16.60	14.75	12.03	11.31	10.95				M4	-7.5	
SCH J16185038-24243205		18.97	16.79	13.63	12.93	12.51	2.34	1.38	0.90	M5	-6.5	
SCH J16190473-23075283		18.50	16.30	13.00	12.34	11.98	2.36	1.47	0.91	M5.5	-12.1	
SCH J16191521-24172429	19.00	17.23	15.19	12.13	11.37	11.05				M4	-13.3	
SCH J16192994-24255414	18.55	16.41	14.53	11.53	10.63	10.22				M4	-6.5	
SCH J16193976-21453527		18.47	16.40	13.22	12.53	12.11	2.10	1.66	0.93	M6	-36.5	DENIS-P J161939.8-214535/M7[e]
SCH J16200756-23591522		19.14	16.75	13.21	12.48	12.05	2.49	1.58	0.92	M6	-24.2	
SCH J16201318-24250155		17.96	16.21	13.77	13.20	12.86				M4	-15.0	
SCH J16202127-21202923		19.14	16.61	13.39	12.74	12.40	2.61	1.62	0.89	M6	-23.9	
SCH J16202523-23160347		19.47	17.59	14.37	13.68	13.23	2.20	1.53	0.88	M5.5	-9.5	
SCH J16211564-24361173		15.86	14.50	12.44	11.81	11.59				M3.5	-5.0	
SCH J16211922-24255250		17.99	15.73	12.17	11.18	10.67				M4	-8.7	
SCH J16212490-24261446		18.24	16.14	12.87	11.86	11.41				M3.5	-6.8	
SCH J16213591-23550341		20.23	17.67	13.94	13.19	12.73	2.38	1.69	0.90	M6	-19.9	
SCH J16221577-23134936		18.87	16.80	13.71	13.14	12.80	2.52	1.55	0.87	M6	-9.2	
SCH J16222156-22173094		18.63	16.52	13.74	13.09	12.61	2.00	1.36	0.92	M5	-60.3	
SCH J16224384-19510575		17.54	15.88	12.35	11.61	11.15	2.42	2.13	0.98	M8	-62.1	

Table 5.1 (cont'd)

ID[a]	g	r	i	J[c]	H[c]	K_S[c]	TiO-7140	TiO-8165	Na-8195	SpType[d]	$W(H\alpha)$ [Å]	Otherid/Sptype
SCH J16235158-23172740		19.86	17.40	13.55	12.89	12.41	2.82	2.16	0.96	M8	-76.8	
SCH J16235474-24383211		19.77	17.21	13.31	12.49	11.92	2.34	1.61	0.95	M6	-12.8	
SCH J16252862-16585055		19.95	17.47	13.67	13.01	12.62	2.66	1.94	0.94	M8	-23.3	
SCH J16252968-22145448		18.64	16.40	13.19	12.49	12.11	2.25	1.41	0.94	M5	-16.2	
SCH J16253671-22242887		19.46	16.97	13.53	12.83	12.45	2.64	1.76	0.93	M7	-11.6	
SCH J16254319-22300300	19.35	17.22	15.84	13.02	12.40	12.09	2.19	1.37	0.90	M5	-9.2	
SCH J16255064-21554577		19.28	17.20	14.26	13.62	13.27	2.36	1.35	0.85	M4.75	-8.9	
SCH J16260630-23340375		19.31	16.85	13.14	12.27	11.75	2.28	1.41	0.93	M5.5	-5.4	
SCH J16262192-24444004		18.98	16.52	12.34	11.48	10.85	2.50	1.83	0.97	M8	-88.8	
SCH J16263026-23365552		19.51	17.48	13.75	12.82	12.21	2.51	1.69	0.94	M6	-32.1	
SCH J16265619-22135224		19.14	16.76	13.48	12.83	12.41	2.71	1.67	0.90	M6	-28.4	
SCH J16270940-21484591		18.39	16.29	12.97	12.15	11.71	1.85	1.27	0.92	M4.5	-11.1	
SCH J16274801-24571371		19.87	17.31	13.54	12.65	12.11	2.20	1.42	0.91	M5	-22.0	
SCH J16281810-24283619		19.19	16.55	12.69	11.81	11.29	2.43	1.49	0.93	M6	-20.1	BKLT J162818-242836[g]
SCH J16284706-24281413		18.71	16.59	13.24	12.53	11.95	2.16	1.72	0.94	M6	-182.7	BKLT J162847-242814[g]
SCH J16292211-17420937	19.23	17.48	15.46	12.58	12.02	11.72	2.17	1.36	0.88	M4.75	-13.0	
SCH J16293625-24565325		18.66	16.43	13.43	12.85	12.48	2.90	1.59	0.86	M6	-41.2	
SCH J16293664-17084094	18.39	16.74	14.82	12.01	11.31	11.01	2.16	1.31	0.91	M4.75	-11.3	
SCH J16293934-16145647	17.35	15.90	14.51	12.19	11.49	11.19				6.3	-3.1	
SCH J16294877-21370914	19.13	17.38	15.45	12.52	11.86	11.52	2.16	1.34	0.92	M5	-9.2	
SCH J16302675-23590905		18.26	16.02	12.61	11.93	11.47	2.39	1.64	0.96	M6	-34.7	
SCH J16303392-24280657		16.67	14.67	11.62	10.76	10.36				M4	-5.3	
SCH J16305349-24245439		17.51	15.51	12.27	11.46	11.04	2.21	1.41	0.97	M5.5	-34.8	
SCH J16310241-24084335		16.70	14.67	11.96	11.24	10.78				M5	-13.5	WSB 68[i]

Table 5.1 (cont'd)

ID[a]	g	r	i	J[c]	H[c]	K_S[c]	TiO-7140	TiO-8165	Na-8195	SpType[d]	$W(H\alpha)$ [Å]	Otherid/Sptype
SCH J16324224-23165644		16.77	14.70	11.76	11.17	10.87	2.60	1.48	0.87	M5.5	-12.9	
SCH J16324726-20593771		18.49	16.55	13.45	12.85	12.47	2.39	1.50	0.91	M6	-25.2	

[a]IDs given in J2000 coordinates.

[b]Two targets observed during the first spectroscopic observing run before the final photometric calibrations were finished do not have calibrated r, i magnitudes.

[c]Near-infrared photometry taken from 2MASS.

[d]Spectral type errors are ± 0.5 for M subclasses.

[e]Reference from: Martín et al. (2004).

[f]Reference from: Preibisch et al. (2002).

[g]Reference from: Barsony et al. (1997).

[h]Reference from: Ardila et al. (2000).

[i]Reference from: Wilking et al. (1987).

5.3 Discussion

5.3.1 HR Diagram for New USco Members

I combine each new member's spectral type and photometry to derive values for its luminosity and effective temperature and place it on a theoretical HR diagram. As described in chapter 2, the final Quest-2 photometry is not on a standard magnitude system. Thus, because of the reliability and uniformity of the 2MASS survey, I chose to use J-band magnitudes and $(J-H)$ colors to derive luminosities. An empirical fit to BC_J as a function of spectral type was determined from the observational data of Leggett et al. (1996) and Leggett et al. (2002) (spectral types M1-M6.5 and M6-L3, respectively). I adopted intrinsic colors, extinction, and effective temperatures using the methods described in Slesnick et al. (2004).

In figure 5.2 I present an HR diagram for the 145 identified low mass members of USco, shown with PMS model tracks and isochrones. The most commonly used PMS models for low mass stars and brown dwarfs are those derived by D'Antona & Mazzitelli (1997) (shown) and Baraffe et al. (1998) which differ primarily in their atmospheric approximations and treatment of convection. Both models suggest similar mass ranges for my data of $0.02M_\odot < M < 0.2M_\odot$, though predicted masses for individual objects can vary by up to $0.07M_\odot$. As illustrated in figure 5.2, I have identified a low mass stellar population of age roughly consistent with the 5 Myr age inferred in previous work on the intermediate mass ($6M_\odot > M > 0.1M_\odot$) members of USco (Preibisch et al., 2002). The mass and age distributions of this population will be discussed further in chapter 6. Among the PMS stars identified in my work, 56 have spectral types M6 or later, and are considered to be brown dwarfs based on theoretical models. Prior to this work, 34 spectroscopically confirmed USco members had been identified at these spectral types (Ardila et al. 2000, Preibisch et al. 2002, Martín et al. 2004), 10 of which are also presented here (see table 5.1). Thus, with this study I have more than doubled the number of known substellar objects in USco.

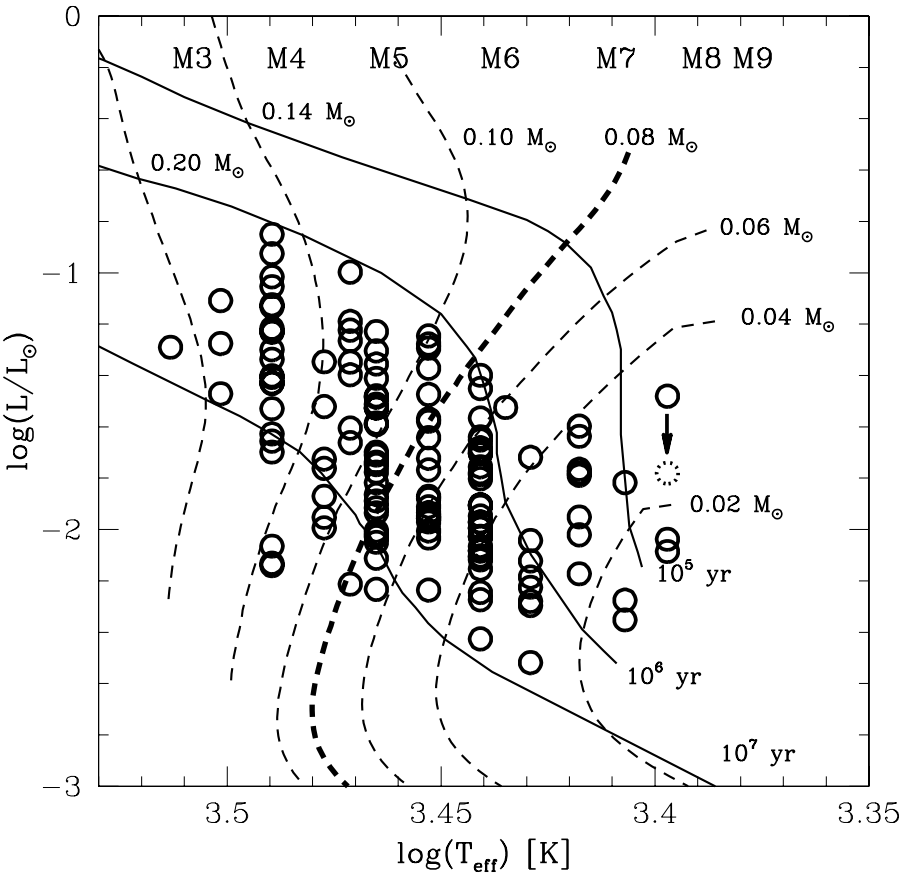

Figure 5.2 HR diagram for new PMS objects found in the USco region, shown with model tracks and isochrones of D'Antona & Mazzitelli (1997). The sample is consistent with an age of ∼5 Myr and contains masses spanning the brown dwarf to stellar regimes. The arrow plus dotted symbol indicates where that star would sit in the HR diagram as a single star if it is an unresolved binary (see §5.3.2).

5.3.2 A Possible Binary

The most luminous M8 brown dwarf (SCH16224384-19510575) is an obvious outlier to the main locus of stars in figure 5.2 appearing overluminous compared to the other sources. This object also has strong Hα emission (see §5.3.3) with a slightly asymmetric profile. It is unlikely that this object is a single, extremely young (<100,000 yr based on HR diagram placement) association member. The object could be a young, PMS-gravity foreground object that happens to fall within my line of sight. The simplest explanation is that SCH16224384-19510575 is an unresolved binary. Assuming typical seeing at Palomar under photometric conditions of $\sim$1.2", any pair with separations $\lesssim$175 AU would not be resolved in my data. If I assume SCH16224384-19510575 consists of 2 equal-luminosity objects, its placement in the HR diagram becomes more consistent with the main locus of association members. This effect is illustrated as an arrow plus dotted symbol in figure 5.2.

5.3.3 Emission Line Objects

The only prominent emission line observed in any of the spectra is Hα which, seen in the spectra of young stars and brown dwarfs, is predominantly created via one of two mechanisms. Weak, narrow Hα lines are presumed to originate from active chromospheres whereas strong, broad and/or asymmetric lines can be produced from high-velocity, infalling accretion or strong winds. Barrado y Navascués & Martín (2003) have proposed an empirical, spectral-type-Hα equivalent width ($W(\mathrm{H}_\alpha)$) relation to describe the upper limit of non-accreting stars and brown dwarfs based on the chromospheric saturation limit observed in young open clusters. Figure 5.3 plots measured Hα equivalent widths for all spectra as a function of spectral type, shown with the Barrado y Navascués & Martín (2003) empirical accretor/nonaccretor division. Many stars and brown dwarfs (see table 5.1) exhibit very strong Hα emission at levels substantially above the accretor/nonaccretor division and thus are possibly still undergoing active accretion.

Because errors on the accretor/nonaccretor division are not well defined (Barrado

y Navascués & Martín, 2003), I determined my own empirical criterion for identifying objects with Hα excess emission. I measured the median values of Hα emission as a function of spectral type (binned by 1 spectral type) using 1-sigma clipping. These values are shown as large magenta X's on figure 5.3. For most bins, I define a star to have an Hα excess if it exhibits emission at a level greater than 3-sigma above the median value for its spectral type (where sigma is defined as the dispersion about the median for all stars used to compute the median value at a given spectral type; shown as magenta –'s on figure 5.3). These sources are boxed in green on figure 5.3. The first and last bins only have 4 and 3 sources respectively. Thus, for these bins I do not have enough measurements to derive a statistically representative value for median Hα emission. Therefore I do not consider any stars in these bins in my sample of Hα excess sources, but note that two M8 stars (including the possible binary discussed in §5.3.2) sit above the Barrado y Navascués & Martín (2003) accretor/nonaccretor dividing line. In general, my empirical criterion for classifying a star as accreting is slightly more conservative (i.e., requires a higher W(Hα)) than the criterion defined by Barrado y Navascués & Martín (2003).

Based on the above criterion, I find 12 objects to exhibit very strong Hα emission. The blue half of the observed spectra for each accreting source is shown in either figure 5.4 or figure 5.5. Two accreting sources lie very close (within $\sim$1 deg) to the young ρOph molecular cloud. However, because ρOph and USco lie at approximately the same distance, if they were escaped, $\lesssim$1 Myr ρOph members we would expect to see them exhibit systematically higher luminosities than USco members of similar spectral type. Based on figure 5.2, this phenomenon is not observed and I include these two stars in my sample of accretors in USco. Thus, I find at an age of $\sim$5 Myr (see chapter 6), 12/145 (or $\sim 8^{+3}_{-2}\%$) of low mass association members (spectral type $\geq$M4) are observed to be accreting based on the strength of Hα emission present in their spectra. In comparison, Guieu et al. (2006) find $\sim 40^{+24}_{-16}\%$ of 1 Myr-old low mass objects in the known subclusters of Taurus to be actively accreting based on the strength of Hα emission observed in their spectra. Thus, a significant fraction of very low mass stars and brown dwarfs must actively stop accreting between 1 and 5

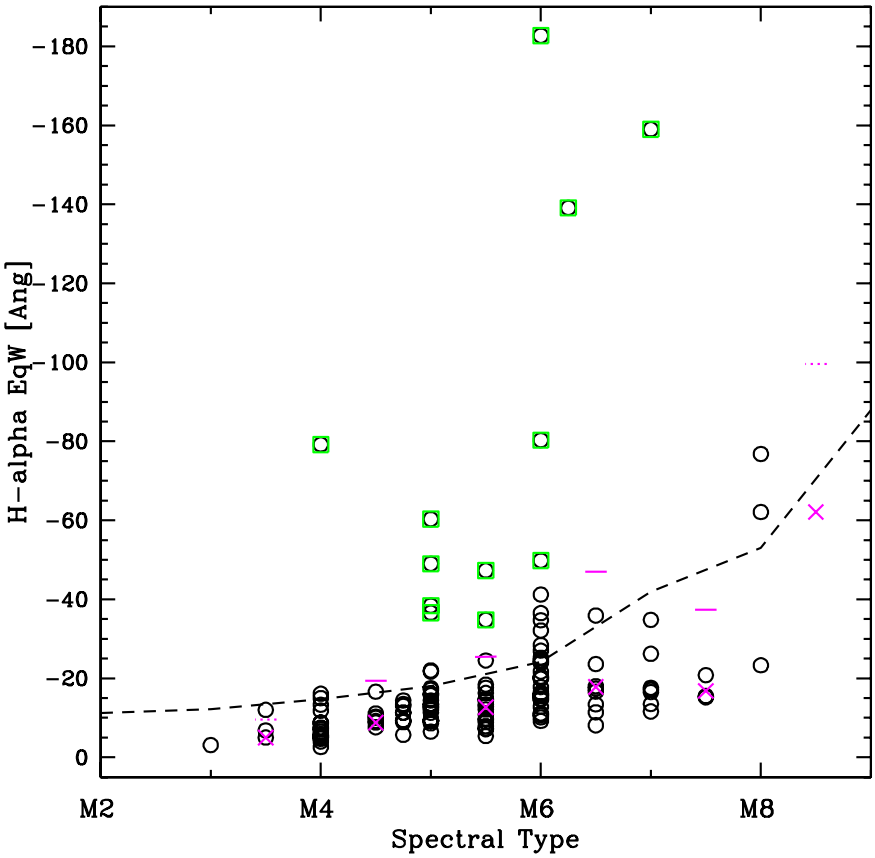

Figure 5.3 Measured Hα equivalent widths for all new USco members as a function of spectral type. The dotted line is the empirical accretor/nonaccretor upper limit derived by Barrado y Navascués & Martín (2003). Magenta X's represent the median $W(H\alpha)$ for each spectral type. Magenta -'s are 3 sigma upper limits above the median. Objects boxed in green are considered to be actively accreting.

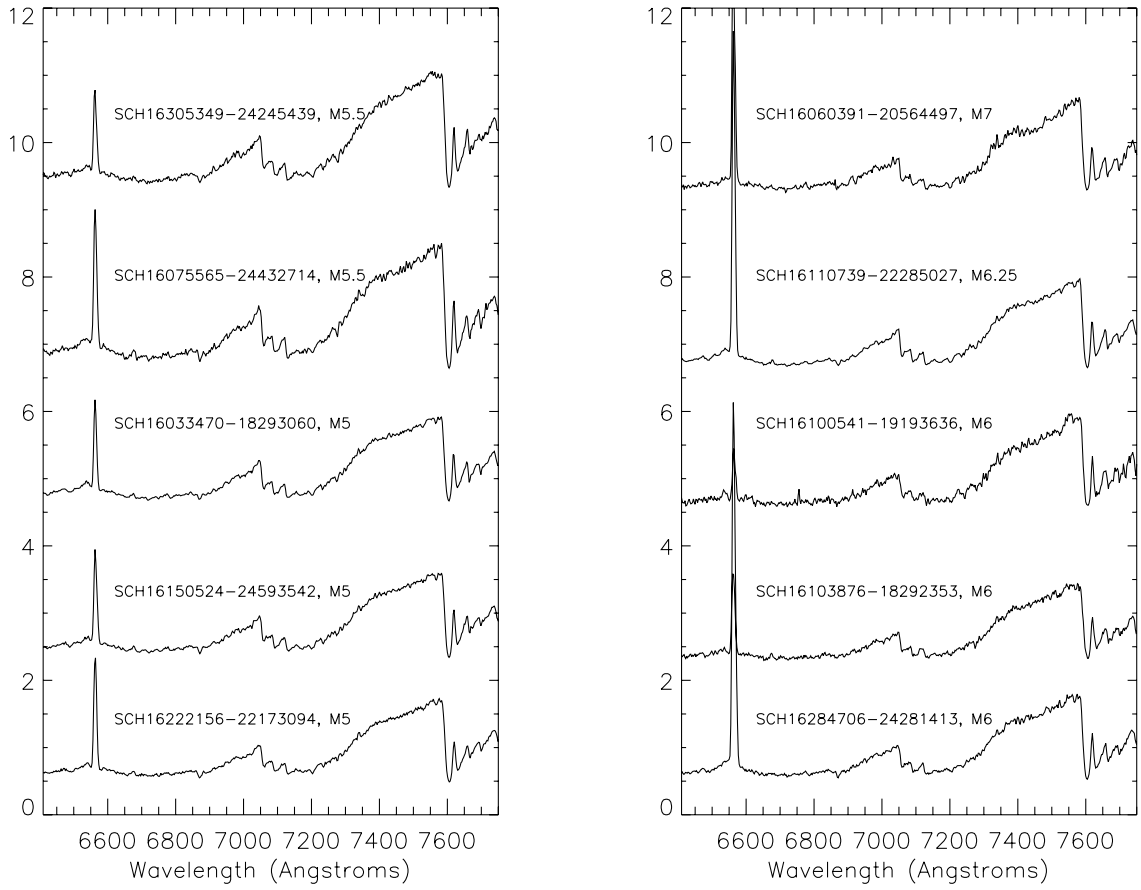

Figure 5.4 Spectra of the 10 stars determined to be accreting (as defined in §5.3.3) that were observed at Palomar, shown in order of spectral type.

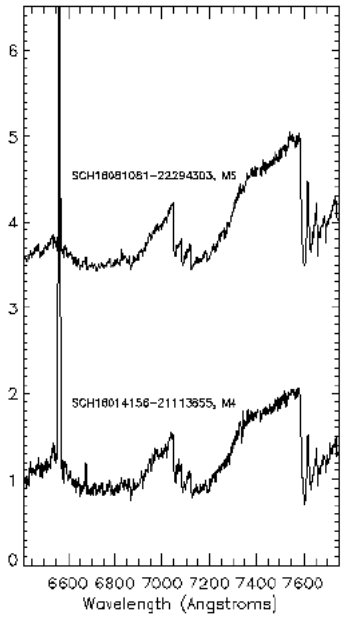

Figure 5.5 Spectra of the 2 stars determined to be accreting (as defined in §5.3.3) that were observed at CTIO, shown in order of spectral type.

Myr. This conclusion is consistent with a median accretion lifetime of ∼2–3 Myr for higher mass stars (Haisch et al. 2001, Hillenbrand 2005).

5.3.4 Spatial Distribution of Low Mass Stars

Figure 5.6 shows the 2D spatial distribution for the 120 known high mass members of USco dentified in the Hipparcos survey. This sample represents the complete population of known members more massive than ∼1 $M_{\odot}$. Thus, I define the boundaries of the Hipparcos stars to represent the boundaries of the USco high mass population. The density of high mass stars is roughly constant from $237 \lesssim \alpha \lesssim 249$ deg and peaks at $\delta \sim$ -24 deg. Contours show the percentage of the 243 spectroscopically observed candidates determined to be bona fide USco members. As can be seen, despite the large area of my Quest-2 survey (shown as a black box), it still only covered a minority of the total association. New members were identified only within the central $\sim 11^o$ in RA and the Northern $\sim 11^o$ in DEC.

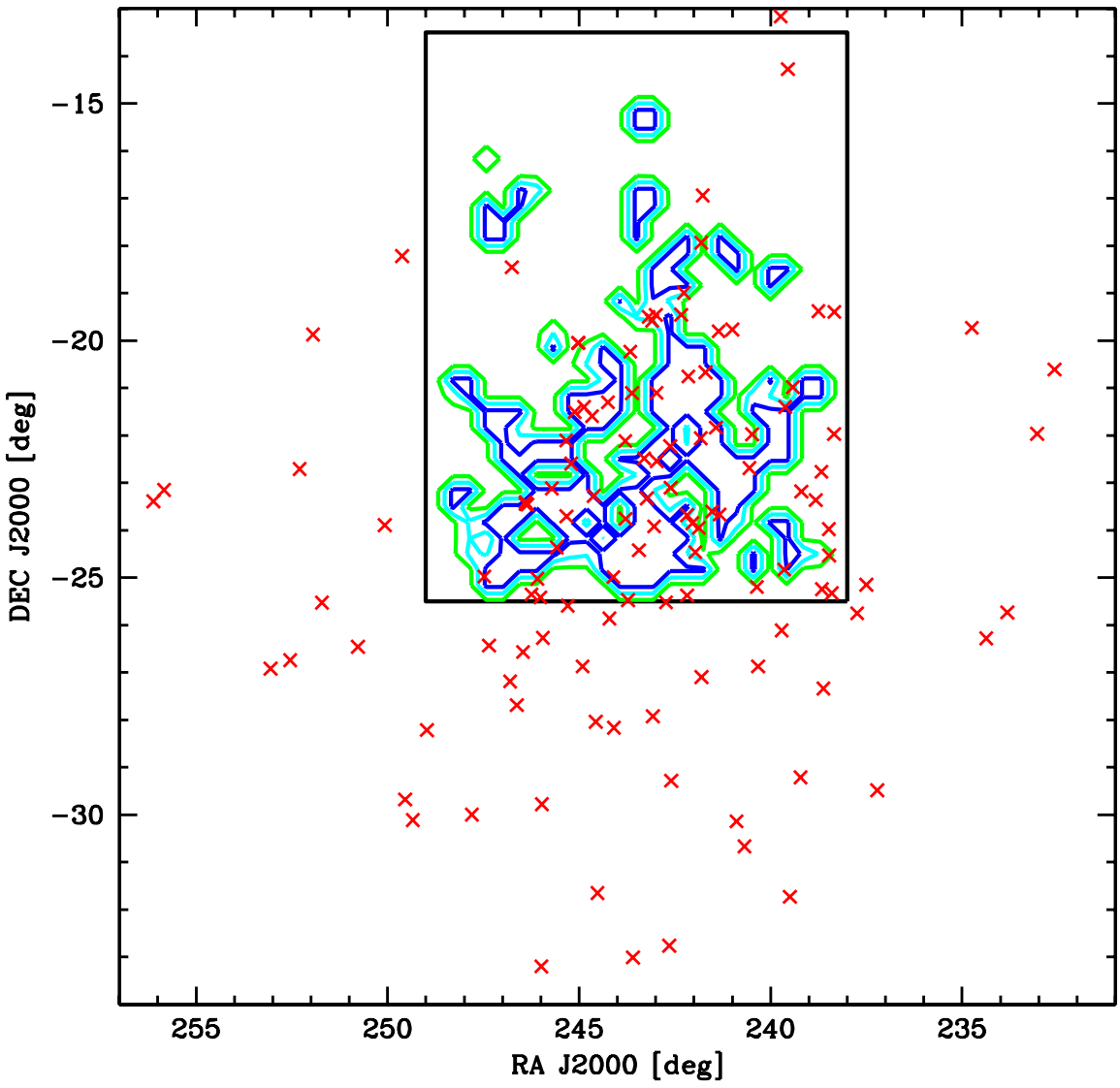

Figure 5.6 Spatial distribution of the 120 known Hipparcos members of USco (red X's) together with a contour plot showing the percentage of Quest-2 candidates observed spectroscopically that were determined to be new low USco members. Contours are shown at 90% (blue), 50% (cyan), and 10% (green) of the peak value. The Quest-2 survey area is shown in black.

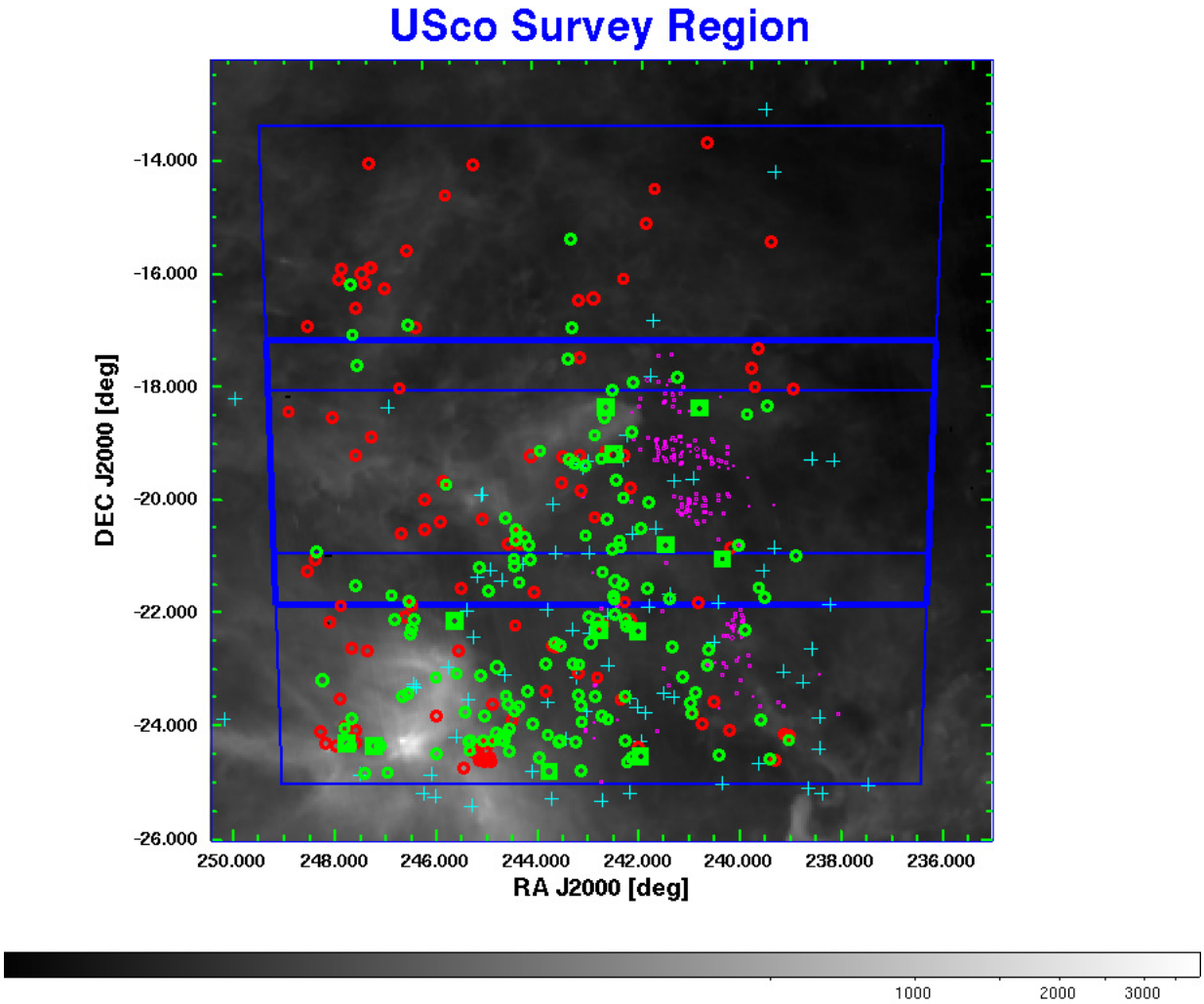

Figure 5.7 Spatial distribution of the USco survey area outlined in blue, overlaid on IRAS 100μm emission. The thicker blue line denotes the outline of the monitoring scan region which was repeated 24 times. New USco members identified from this work (145; green circles) are shown with previously known, spectroscopically confirmed low mass members (196; Sp Type $\geq$K7 corresponding to M $\leq$0.6 $M_{\odot}$ at 5 Myr; small magenta circles) from the literature (see text), high mass Hipparcos members (120; cyan pluses) and spectroscopic targets determined to be field dwarfs (98; red circles). The 12 new members which exhibit Hα excess emission are boxed.

Figure 5.7 shows the spatial distribution of observed spectral candidates overlaid on an IRAS 100μm emission map. New USco members identified from this work are shown with previously known, spectroscopically confirmed low mass members from the literature, high mass Hipparcos members and spectroscopic targets determined to be field dwarfs. The 12 new members that exhibit Hα excess emission are boxed. In general, the low mass PMS stars presented here share a common spatial distribution with the high mass Hipparcos members. Efforts to observe northwest of the Hipparcos stars largely yielded reddened field dwarfs rather than young association members. Figure 5.8 shows 1D spatial distributions for the 145 low mass association members discussed here (green line), together with those for the 56 Hipparcos stars that fall within my survey area (black line). The densities of both populations fall off sharply from -24^o at the association center to its northern edge. Figures 5.9 and 5.10 show histograms as a function of RA (figure 5.9) and DEC (figure 5.10) of the total number of candidates observed spectroscopically compared to the number determined to be bona fide USco members. Bottom panels show the percentage of observed candidates determined to be USco members as a function of RA and DEC. From figure 5.8, I conclude that the density of low mass association members found in the Quest-2 survey peaks at α $\sim$242^o and δ $\sim$ -25^o with stellar densities falling off beyond these values. Based on figures 5.6 and 5.10, my survey extended past the association's edge only at its northern boundary, which occurs at $\sim$-15^o (see figure 5.10).

5.4 Summary

I have completed a large-area *gri* photometric survey in and near the Upper Scorpius region of recent star formation. From these data I selected candidate new PMS association members based on their optical and near-infrared colors and magnitudes. I present in this chapter results from my spectroscopic follow-up campaign. I observed a total of 243 candidates at either Palomar or CTIO, and determined 145 ($\sim$60%) to be bona fide new Upper Scorpius members. I derive an HR diagram for new members and identify a possible unresolved binary. I measure Hα emission for all new members

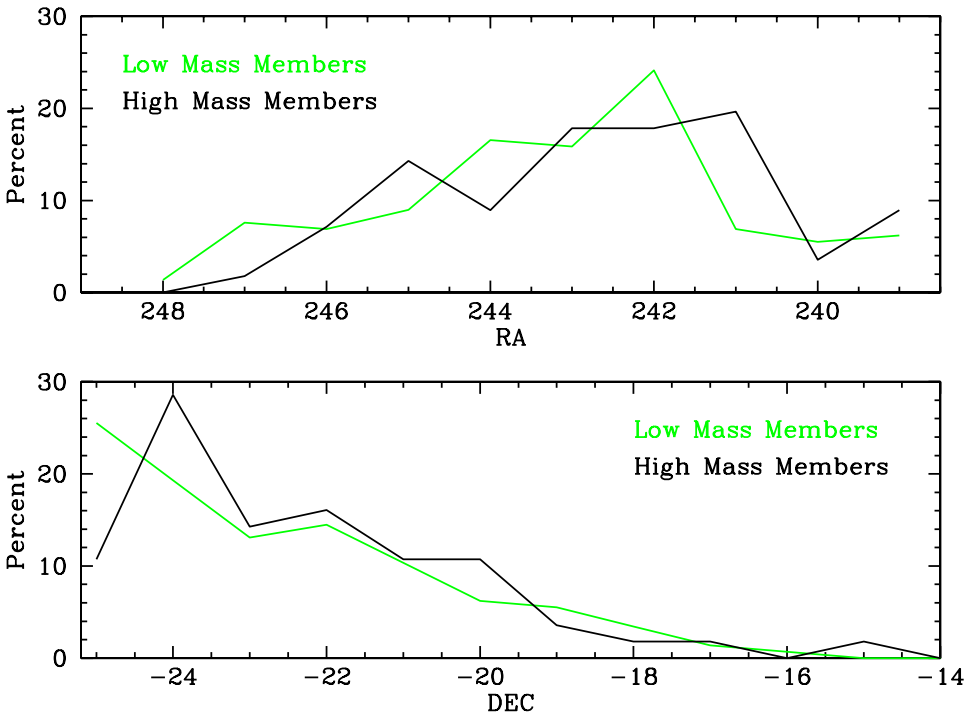

Figure 5.8 Top panel shows the percentage of the 145 low mass stars discussed in this work that lie at a given RA (green) together with same information for the 56 high mass Hipparcos stars found in the Quest-2 survey area (black). Bottom panel illustrates the same information as a function of DEC.

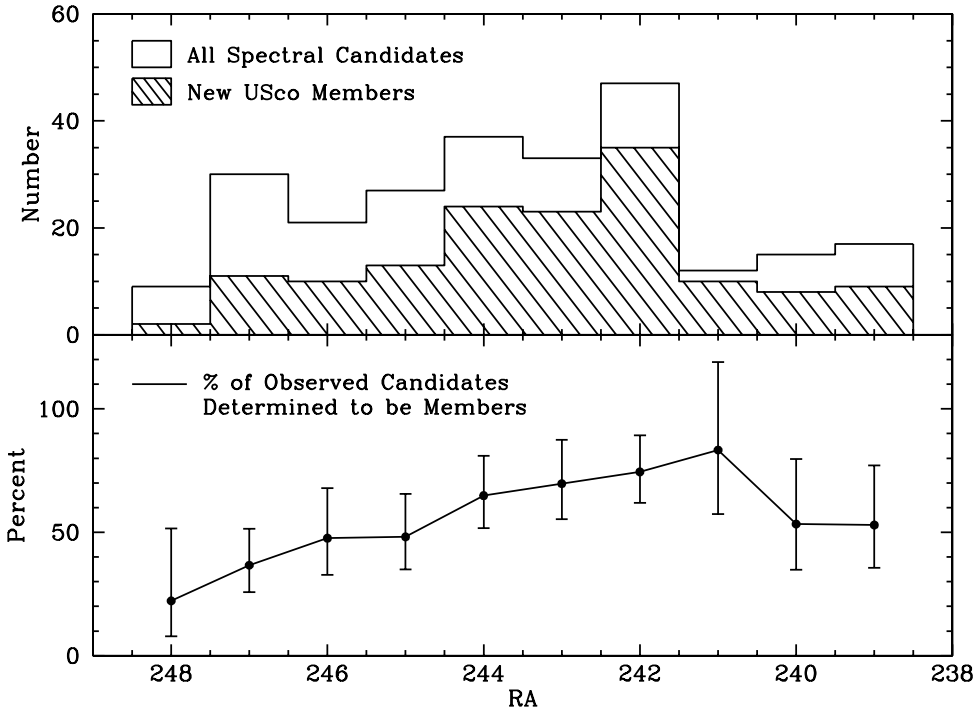

Figure 5.9 Top panel contains a histogram of RA values for all candidates in USco observed spectroscopically (open histogram) and for those observed candidates determined to be bona fide members (hatched histogram). Bottom panel shows the percentge of observed candidates determined to be USco members as a function of RA.

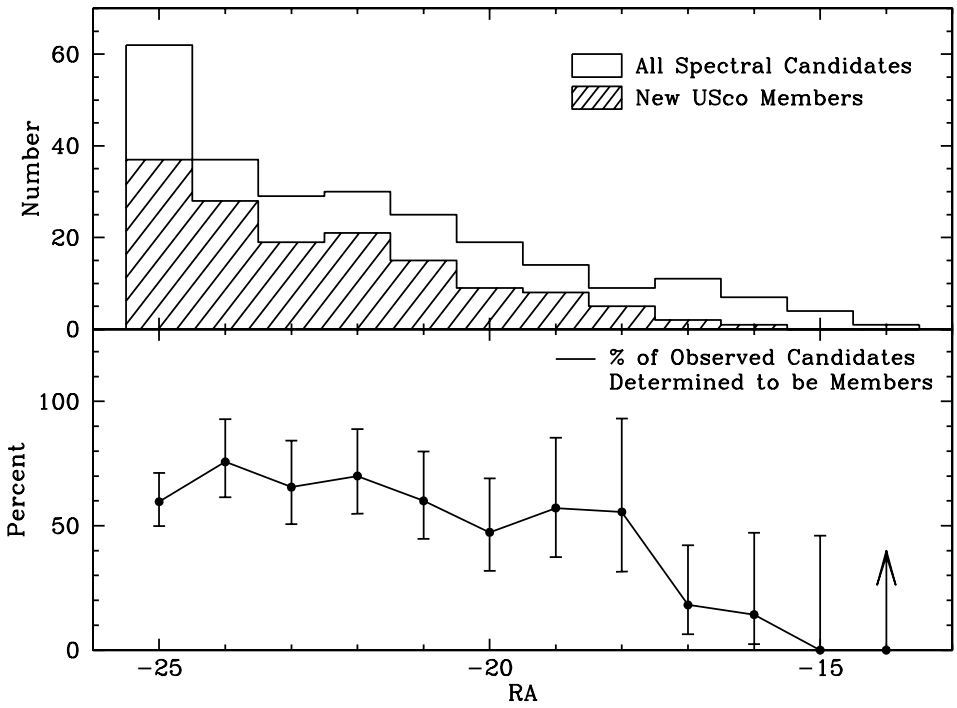

Figure 5.10 Top panel contains a histogram of DEC values for all candidates in USco observed spectroscopically (open histogram) and for those observed candidates determined to be bona fide members (hatched histogram). Bottom panel shows the percentage of observed candidates determined to be USco members as a function of DEC. The right-most point at DEC=-14 is drawn as an arrow because 0 out of 1 observed stars were determined to be PMS stars. Thus, due to small number statistics, the errorbar is larger than the plot.

and determine 12 of the 145 low mass stars and brown dwarfs in the 5 Myr USco association are still accreting. Based on comparison of the spatial distributions of low and high mass association members, I find no evidence for spatial segregation in USco within the northern portion of the association.